Longitudinal and normal electroconvection rolls in a nematic liquid crystal with positive dielectric and negative conductivity anisotropy

Jana Heuer and Ralf Stannarius
Otto-von-Guericke-University, Institute of Experimental Physics, Universitätsplatz 2, 39106 Magdeburg, Germany

Maria-Gabriela Tamba and Wolfgang Weissflog
Martin-Luther-University, Institute of Physical Chemistry, Mühlpforte 1, 06108 Halle, Germany

(Received 1 November 2007; published 12 May 2008)

We study electroconvection patterns that appear above the splay Fréedericksz transition in a bent-core nematic liquid crystal with positive dielectric and negative conductivity anisotropy. In contrast to most of the previously observed convection rolls in nematics, they are not shadowgraph patterns at onset. Unusual effects are observed like a transition between longitudinal and normal rolls, controlled by the excitation frequency, as well as a voltage dependent reorientation of the convection rolls in a metastable domain. We present experimentally determined pattern state diagrams for planar alignment and characterize the patterns optically.

DOI: 10.1103/PhysRevE.77.056206 PACS number(s): 05.45.−a, 61.30.−v, 47.54.−r, 83.80.Xz

I. INTRODUCTION

Electrohydrodynamic convection (EHC) of nematic liquid crystals is a well suited system to study pattern formation in anisotropic fluids. It is driven electrically and yields a large variety of spatially extended patterns with different dynamics. EHC in calamitic (rodlike) nematic liquid crystals has been studied experimentally for a long time (e.g., [1,2] for an overview). Several studies have dealt, for example, with the optical observation via shadowgraph method [3–5], spatiotemporal characterization [6–8], traveling waves [9–11], oblique [12,13], as well as abnormal rolls [14–16]. A model based on the Carr-Helfrich mechanism has been developed that describes underlying physical processes leading to the instability. The basic model [17,18] has been generalized for ac excitation [19], and extended to the weakly nonlinear case in the form of Ginzburg-Landau equations [20]. Potential non-Ohmic contributions to the conductivity have been considered, leading to the weak electrolyte model (WEM) [21]. In [10] the equations for the WEM were written down in a usable form and predictions were compared with experiment.

In novel liquid crystal materials with unconventional material parameters, new types of electroconvection patterns have been found (for an overview, see Ref. [22]). Some of them can be explained by the Carr-Helfrich effect, while other structures require modifications and extensions, like the inclusion of flexoelectric coefficients and WEM effects. In particular, the combination of the signs of the dielectric anisotropy $\Delta\varepsilon$ and the conductivity anisotropy $\Delta\sigma$ play a decisive role for the type of convection pattern that is selected. The conventional electroconvection experiments regard mesogens with negative $\Delta\varepsilon$ and positive $\Delta\sigma$. In the following, the notation $(-,+)$ will be used, where the first character refers to the sign of the dielectric anisotropy and the second one to the sign of the conductivity anisotropy. In several recent studies, where different combinations of both signs have been considered, novel patterns or bifurcation scenarios have been found, e.g., for the $(+,-)$ [23–25], $(+,+)$ [26,27], $(-,-)$ cases [28–30]. Whereas for the first two cases, Carr-Helfrich type mechanisms can be employed as an explanation, the last type requires the inclusion of other terms and processes, like flexoelectric contributions. We refer to the first types as "standard EHC". In the definition of the "standard model" we follow Ref. [29] and consider all instability mechanisms that follow the Carr-Helfrich model, including its extensions to three dimensions and to ac. The weak electrolyte model [21] and flexoelectricity are excluded.

The mesogen studied in the present publication is a bent-core compound with positive $\Delta\varepsilon$ and negative $\Delta\sigma$, $(+,-)$. In planar alignment it develops unconventional electroconvection patterns above the splay Fréedericksz transition, e.g., longitudinal rolls that are oriented parallel or nearly parallel to the initial director $\mathbf{n}_0$ (for a description of the Fréedericksz transition, see, e.g., Ref. [31] and Sec. III here). This is in contrast to the classical normal rolls with an orientation perpendicular to $\mathbf{n}_0$ in the $(-,+)$ case in accordance with the standard model (see [23]). A mechanism leading to the formation of longitudinal rolls at electric fields above the Fréedericksz transition has been introduced and explained within a basic model [24]. Therein, a periodic twist modulation is constitutive for the longitudinal patterns that are described as standard EHC. Irrespective of the different convection mechanisms and signs of the anisotropies, these patterns exhibit many optical similarities to those described in Refs. [23,28–30], in particular with respect to their orientation parallel to the initial director orientation. Like the longitudinal patterns described here and in Ref. [24], the parallel nonstandard patterns investigated in Refs. [28,29] and the parallel patterns observed in another bent-core nematic [30] do not produce shadowgraph patterns near the convection threshold. Buka *et al.* [23] have studied a calamitic nematic with $(+,-)$ material parameters, and similar to our situation, parallel EHC rolls have been found above the Fréedericksz threshold. But since their observations were not performed under crossed polarizers, it is not clear whether the shadowgraph observed there was preceded by interference textures at lower voltages. The authors of Ref. [23] mention, however, some unspecific convection below the shadowgraph pattern onset, which suggests that the material develops simi-

lar structures as described in Ref. [24] and here.

Despite some common optical features, the origin of the different patterns mentioned above is diverse because the sign of $\Delta\varepsilon$ is negative in the materials studied in Refs. [28–30] whereas it is positive in Refs. [23,24] and in this work. As said before, the standard EHC model does not work for (−,−) materials, nonstandard models that include flexoelectricity have therefore been developed [32].

Onset of electrohydrodynamic convection patterns in nematics above the Fréedericksz threshold has been observed in another geometry as well: In homeotropic cells, patterns of materials with positive conductivity anisotropy can occur above a bend Fréedericksz transition [33–35]. However, owing to the different nature of this homeotropic geometry and to the different combination of signs of the dielectric and conductivity anisotropies, these structures and instability mechanisms cannot be directly related with the patterns described here. In the homeotropic geometry, the Fréedericksz transition practically establishes a nearly planar orientation of the director in the cell middle, so that the classical convection mechanism as in (−,+) materials can become effective. Note that in the (+,−) type material investigated in this study, one has EHC in homeotropic cells without preceding Fréedericksz transition [36].

In this publication, we present an experimental characterization of different pattern types, in a (+,−) compound. The basic features of this type of instability have been described earlier [24]. Here, we present a detailed investigation of the instability for different excitation frequencies. The conductivity anisotropy as a decisive material parameter is measured and the role of temperature changes on the onset and orientation of the patterns is studied. We find, for example, a transition from longitudinal to normal rolls depending on the excitation frequency, as well as a temperature dependent transition between both orientations. An unconventional feature of the observed bent-core material is the formation of a metastable ground state in planar cells that has not been fully understood so far. We describe the convection patterns in that metastable domain, in particular a field induced transition from longitudinal rolls to normal convection rolls.

In order to compare experimental results with the predictions in Ref. [24], a brief introduction of the model therein is necessary. A small initial fluctuation is considered that is a periodic modulation of the director, with a wave vector perpendicular to $\mathbf{n}_0$ (Fig. 1). This twist mode does not grow from the undistorted ground state $\mathbf{n} \equiv \mathbf{n}_0$ but from a uniformly distorted state, i.e., a homogeneous tilt out of the *x*-*y* plane that is realized in experiments by the splay Fréedericksz transition.

The periodic deflections of the director out of the tilt plane cause a spatially modulated charge transport and a charge segregation in the *y* direction, in the same way as periodic tilt deflections in the classical Carr-Helfrich structures lead to a charge segregation along *x*. This modulated charge couples via Coulomb forces to the external electric field and leads to a shear flow of the nematic sample in convection rolls that are oriented along the initial director. In principle, it should be possible with some efforts to calculate the threshold for this convection mechanism with the complete three-dimensional set of equations for the director, flow, and charge fields. In [24], a simpler ansatz has been used to demonstrate the principal instability mechanism. The stability of the tilted, in-plane homogeneous ground state has been tested within a one-dimensional model, i.e., the particular director profile in the *z* direction is not considered. This model yields some specific conditions for the conductivity and viscous parameters of the material which are necessary for the instability to occur. These conditions (a combination of a negative conductivity anisotropy with a positive viscosity coefficient α_3) seem to be fulfilled in particular in materials which are close to a nematic-smectic transition. A pattern with a wave vector perpendicular to the *x* direction and to $\mathbf{n}_0$ is produced.

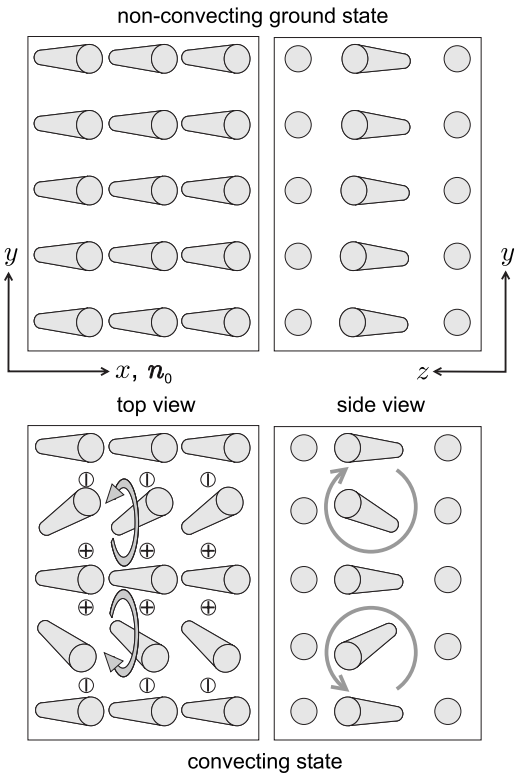

FIG. 1. Top view (left) and side view (right) of the director configuration assumed in Ref. [24]. Top: homogeneously tilted ground state; bottom: periodic modulation. The cylinders symbolize the locally preferred director configuration. The director alignment at the plates is $\mathbf{n}_0$. *x*-*y* is the cell plane, *z* is normal to the cell.

II. SETUP AND COMPOUND

The nematic liquid crystal is sandwiched between two parallel glass plates that are coated with transparent indium-tin-oxide electrodes and with a rubbed polyimide layer for a planar director alignment in the *x* direction (Fig. 2). Thus the initial director orientation $\mathbf{n}_0$ is along *x*. The cell gap *d* is 25 μm. A sinusoidal electric field is applied along the *z* direction. The temperature is controlled with a Linkam heating stage and set to 4 K below the transition temperature T_{iso} if not otherwise stated. The textures are observed with a polarizing microscope in transmission (Zeiss Jenapol D), contrast has been enhanced in most pictures shown below.

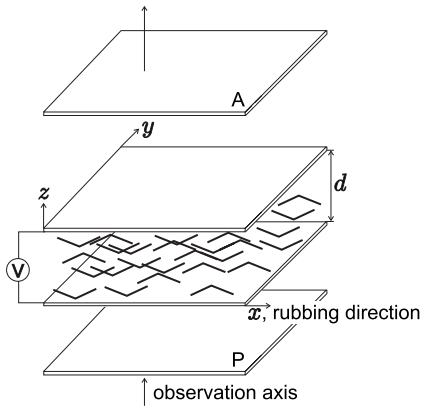

FIG. 2. Sketch of the setup with analyzer A and polarizer P. The cell gap is d.

We note that different experimental runs have been performed within a time period of several months and with different cells. Because the absolute value of the conductivity is different for individual cells and has certain long-term trends in each cell, the absolute values for transition frequencies and threshold voltages may differ for different measurements.

The mesogen GTP 240 studied here contains a bent-core mesogenic unit that is connected to a calamitic unit by a spacer [37], Fig. 3. This is one of the possible chemical techniques to incorporate bent-core mesogenic structures in nematogens. The phase sequence is: crystalline 160 °C (smectic C 149 °C) nematic 167.5 °C isotropic. The smectic C phase is monotropic, it appears only during cooling.

III. MEASUREMENT OF ANISOTROPIES

As stated in the Introduction, the combination of the signs of dielectric and conduction anisotropies is crucial for the character of the electrohydrodynamic instability. Thus knowledge of at least the signs of $\Delta\varepsilon$ and $\Delta\sigma$ is a precondition for the interpretation of the convection mechanism.

EHC of the investigated mesogen in planar alignment is preceded by a splay Fréedericksz transition. The existence of this splay type transition evidences that the dielectric constant $\Delta\varepsilon=\varepsilon_{\parallel}-\varepsilon_{\perp}$ is necessarily positive [31] (indices $\parallel$ and $\perp$ refer to the director $\mathbf{n}$).

The sign of the conductivity anisotropy $\Delta\sigma=\sigma_{\parallel}-\sigma_{\perp}$, and in rough approximation an absolute value of this anisotropy, can be determined from independent experiments. We have chosen electric field dependent current measurements and record the voltages U_{cell} and U_{R_0} of the nematic sandwich cell and of a serial reference resistance $R_0=100$ kΩ, respectively, at an excitation frequency $f_0=1$ kHz. Strictly, the impedance is a complex quantity since the cell represents a parallel circuit of Ohmic and capacitive elements. In our material, however, the Ohmic conductivity is rather high and we can neglect capacitive contributions. Figure 4(a) (circles) shows the measured effective conductivity $\sigma_{\mathrm{eff}}=[d/(R_0A)](U_{R_0}/U_{\mathrm{cell}})$ as a function of the voltage U_{cell}, with the electrode area $A=1$ cm$\times 1$ cm and the cell gap $d=25$ μm at $T-T_{\mathrm{iso}}=-0.5$ K. Below the Fréedericksz transition (FT, dash-dotted line) the director remains in the untilted ground state, the relevant component of the conductivity tensor is $\sigma_{\perp}$, the effective conductivity is practically constant. σ_{eff} decreases above the Fréedericksz transition, where the director changes gradually from a perpendicular to a more parallel alignment with respect to the applied electric field [see the inset sketches in Fig. 4(a)]. The optical visibility of the Fréedericksz transition in the polarizing microscope (see

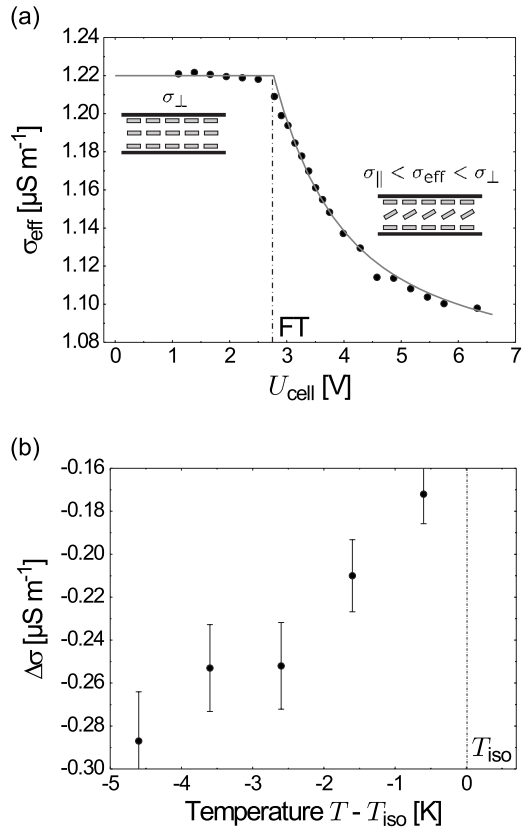

FIG. 4. (a) Dependence of the effective conductivity σ_{eff} on the voltage U_{cell}. Below the Fréedericksz transition (FT, dash-dotted line) the measured conductivity corresponds to the conductivity perpendicular to $\mathbf{n}$ (inset sketch on the left). Above the FT, the effective conductivity contains contributions of both, $\sigma_{\parallel}$ and $\sigma_{\perp}$ (inset sketch on the right). (b) $\Delta\sigma$ for different temperatures. Transition temperature T_{iso} between nematic and isotropic phase is marked. A systematic error of all $\Delta\sigma$ to larger values because of unknown K_{33}/K_{11} and $\varepsilon_{\parallel}/\varepsilon_{\perp}$ ratios is not included here.

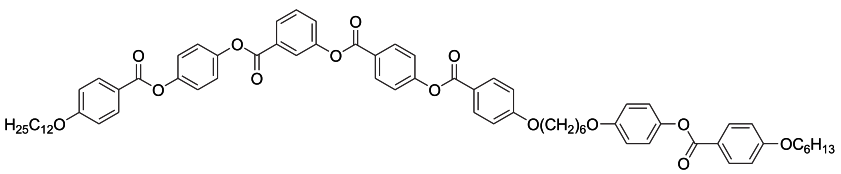

FIG. 3. Chemical structure of GTP 240.

Ref. [25]) coincides with the kink of σ_{eff}. For larger values of U_{cell}, σ_{eff} should further decrease and finally saturate to $\sigma_{\parallel}$, but this value has not been reached in our experiment because the director does not reach the asymptotic normal orientation before the convection sets in. In order to obtain reproducible results, we start the current measurements after the cell has been exposed to a low amplitude ac voltage for several hours.

From the measured values we can already conclude that $\Delta\sigma=\sigma_{\parallel}-\sigma_{\perp}<0$. For a more quantitative analysis we calculated the expected $\sigma_{\text{eff}}(U_{\text{cell}})$ in consideration of the resulting resistance as an infinite serial connection of infinitesimally small resistances:

$$\left[\frac{1}{d}\int_0^d \frac{dz}{\sqrt{\sigma_{\parallel}^2 \sin^2 \phi(U_{\text{cell}};z)+\sigma_{\perp}^2 \cos^2 \phi(U_{\text{cell}};z)}}\right]^{-1}.$$

The director deflection $\phi(z)$ can be calculated as the inversion of the elliptic integral for U_{cell}, with the voltage U_{F} at the Fréedericksz transition [31]. The model for this fit contains several rough approximations. First, we use the constant electric field $E=U_{\text{cell}}/d$ as an approximation for the actual z-dependent electric field. Second, we apply the elastic approximation: $K_{11}=K_{33}=K$ for the elastic splay and bend constants K_{11}, K_{33}, and assume $\varepsilon_{\parallel}\approx\varepsilon_{\perp}$. Actually, we expect from earlier, independent measurements that $K_{33}>K_{11}$, and the existence of the Fréedericksz transition evidences that $\varepsilon_{\parallel}>\varepsilon_{\perp}$. Both inequalities have the effect of moderating the director deflections above the threshold, i.e. the fit parameter $\sigma_{\parallel}$ is systematically overestimated with our approximations. Since no quantitative data on the dielectric and elastic anisotropies exist, we can only estimate that all $\sigma_{\parallel}$ obtained from the fits are systematically larger than the actual values, i.e., the absolute values of $\Delta\sigma$ may be underestimated by 10–20 %. The solid grey line in Fig. 4(a) represents the fit with $U_{\text{F}}=2.77$ V, $\sigma_{\perp}=1.22$ μS m^{-1} and $\sigma_{\parallel}=1.05$ μS m^{-1}. Thus for $T-T_{\text{iso}}=-0.5$ K the anisotropy of the electric conductivity is determined to be $\Delta\sigma=-0.17$ μS m^{-1} and $\Delta\sigma/\sigma_{\perp}=-0.14$, correspondingly. Actually, the model curve is correct only for the limits $U<U_{\text{F}}$ and $U\gg U_{\text{F}}$, but the qualitative characteristics is reproduced also for intermediate fields.

The variation of $\Delta\sigma$ with increasing temperature is depicted in Fig. 4(b). An increasing trend is obvious, i.e., the absolute value of $\Delta\sigma$ is highest near the transition to the smectic C phase at lower temperatures and decreases for higher temperatures. At the transition temperature T_{iso} to the isotropic phase, $|\Delta\sigma|$ is minimal. Note that there is no sign inversion of $\Delta\sigma$ in the interesting temperature range.

IV. CHARACTERIZATION OF THE PATTERNS

The basic properties of the patterns observed at onset have been described earlier [24]. The following Sec. IV A contains a detailed characterization of the longitudinal pattern observed at threshold and texture changes above threshold related to increased driving voltages. In Sec. IV B we investigate the dynamics of the director field in the longitudinal pattern and show that they can be classified dynamically as the conduction pattern type in standard EHC. Qualitative structural changes as a consequence of the variation of excitation parameters (frequency, voltage) and sample temperature are analyzed in Sec. IV C. In particular, patterns with different wave vector orientations can be observed when the driving parameters are varied, as in classical EHC (cf. oblique rolls). In Sec. V, we discuss pattern formation in a so far not fully understood metastable ground state of the material in the planar cell.

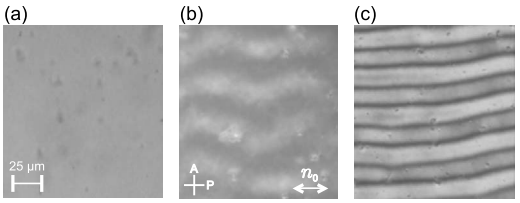

FIG. 5. Polarizing microscopy images of longitudinal rolls (a) without polarizers at $U\approx U_{\text{c}}$, (b) crossed polarizers (A, P), $U\approx U_{\text{c}}$, (c) crossed polarizers, $U=1.04\ U_{\text{c}}$. The initial director orientation $\mathbf{n}_0$ is marked, $f_0=1$ kHz, $U_{\text{c}}=6.5$ V.

A. Longitudinal rolls

Over a large parameter range in the nematic phase, the (+,−) bent-core mesogen exhibits longitudinal rolls at pattern onset when exposed to sufficiently strong ac fields. These rolls are roughly oriented parallel to the initial director orientation $\mathbf{n}_0$ [Figs. 5(b) and 5(c)]. This is in contrast to classical EHC in the planar (−,+) case, where the rolls are oriented perpendicular to $\mathbf{n}_0$ or slightly tilted with respect to the perpendicular direction (normal or oblique rolls). Furthermore, the longitudinal convection rolls do not produce detectable shadowgraph patterns near the threshold voltage U_{c} [Fig. 5(a)], i.e., at pattern onset the rolls are only visible with two polarizers. Thus the longitudinal rolls at onset must be interference patterns. In contrast to the shadowgraph patterns that appear at a few percent above the threshold voltage [Fig. 5(c)], the image is generated only by the modulation of the optical phase profile of ordinary and extraordinary waves, while focusing effects are negligible.

A short discussion of the optical characteristics of the patterns is needed here. The classical electroconvection patterns, irrespective of whether they are observed in planar or homeotropic cells, lead to a spatial modulation of the director tilt angle in the sandwich cell. The director tilt denominates the deflection out of the cell plane, the tilt plane is perpendicular to the cell plane. This modulation is connected with a spatial variation of the effective refractive index for normally incident light polarized with the electric field in the director tilt plane. When the convection patterns are observed without polarizers, the shadowgraph texture appears as a consequence of light focusing. This effect is observable as well, when a polarizer is inserted in the direction of the surface director orientation of a planar cell. However, it is absent when the polarizer is normal to the director tilt plane. In that case, the ordinary refractive index is effective and the light passes the cell unmodulated unless the director possesses an out-of-plane component, as, e.g., in chevron tex-

tures [38]. The finding that shadowgraph effects are absent near the onset of the convection patterns in our material evidences that the tilt angle and thus the effective refractive index are not, or only weakly, modulated in the cell plane. This means optically that the intensity of transmitted light is not modulated, and light passes the cell without measurable deflection.

The director tilt is thus almost uniform in the cell plane. Above the splay Fréedericksz threshold, the tilt angle increases with increasing voltage. The change of cell birefringence above this threshold but below EHC onset can be used as a rough measure of the tilt deflection magnitude. In the 25 μm cells studied here, the birefringence at voltages near the EHC onset has dropped to about 1/2 of its initial maximum value in zero field. We can conclude that the tilt angle profile is still far from being saturated when EHC sets in.

The periodic longitudinal convection pattern is observable near onset with two polarizers. This can be explained when the ellipticity and/or polarization plane of the transmitted light is modulated in the cell plane. The consequences of a twist deflection of the director field for the optical transmission in EHC have been analyzed earlier [7,16,38,39]. If an in-plane uniformly tilted director field is twisted out of the tilt plane in the cell middle (cf. Fig. 1, bottom right), the Mauguin limit guarantees in thick cells that the polarization direction of linearly polarized incident light is adiabatically guided with the twist. Thus the polarization direction rotates back to the direction of the incident wave after passing the cell, in first order approximation. The polarization state of the incident light is reestablished and the twist does not affect the optical texture. A perturbation of these linearly polarized eigenmodes is allowed for by so-called leakage modes. They introduce a slight ellipticity of the light passing the twist deflected director field. These leakage modes are responsible for a periodic spatial modulation of ellipticity of the transmitted light, which can be visualized, for example, by the analyzer inserted orthogonally to the polarizer. This configuration does not distinguish between left-handed and right-handed twist, but gives a contrast between nontwisted and twisted regions of the director field in the convection pattern, with twice the wave vector of the flow and director patterns. An even better contrast can be achieved when the polarizers are slightly decrossed, or when a phase plate is inserted into the optical path [7,38,39]. In that case, the spatial wave number of the optical pattern halves, and it becomes equal to the convection pattern wave number.

The model derived in Ref. [24] yields patterns that will not produce shadowgraph patterns at onset, because the z component of $\mathbf{n}$ is not modulated in the cell plane. As discussed above, such patterns will only be detectable between two polarizers. Hence the features predicted by the model agree with our experimental observations: the longitudinal orientation as well as the optical appearance as interference patterns. The model also explains the pattern onset above the Fréedericksz threshold.

B. Pattern dynamics

Reference [24] makes no prediction about the pattern dynamics under ac excitation. Standard electroconvection produces three different dynamic regimes in ac electric fields [8]. Conduction roll textures are stationary, i.e., the director configuration is only weakly time dependent, while the charges alternate with the excitation field. The textures of dielectric rolls change in time with the period of the excitation, they are characterized by a nearly stationary charge field. At certain excitation wave forms, subharmonic structures can occur that exhibit a dynamics with the double excitation period [8]. The model in [24] describes only the dc case of the twist mode destabilization and thus the related optical patterns are stationary. In ac fields, we expect from analogy considerations that similar dynamic regimes exist as in the classical case. With this assumption, the dynamics structures under low frequency excitation should be analogous to classical conduction patterns. The dynamics of the longitudinal patterns under ac fields in the experiments of the present study shows the appropriateness of these suppositions.

In order to detect oscillations of the pattern, an image sequence has been generated by means of a high speed camera with a frame rate of 2000 fps, while the EHC patterns have been excited with an ac frequency of $f_0=500$ Hz. The complete data set in two spatial dimensions and time has been three-dimensional (3D) Fourier transformed into the wave vector-frequency space. The 3D spatiotemporal spectrum indicates that the pattern is stationary, i.e., there are only peaks at $f=0$ in the frequency domain. In particular, there are no measurable peaks at f_0 or $2f_0$. Hence in its dynamic behavior the longitudinal pattern is similar to the standard conduction regime. We have not observed any qualitative change of the dynamics at lower or higher frequencies in the complete range investigated.

Figure 6(a) shows an exemplary picture from the image sequence that has been Fourier transformed. The two-dimensional Fourier spectrum in spatial coordinates in Fig. 6(b) has been obtained from a cut of the above mentioned 3D FT (square root of the power spectrum) at $f=0$. This plane contains the time averaged contribution to the amplitude spectrum. The wave numbers $q_{x/y}$ are scaled with $q_d=2\pi/d$ corresponding to the cell gap d. The total intensity peak at $q_x=q_y=0$ has been set to zero. Signals appear only on the q_y axis near $q_x=0$ at 0.59 q_d, 1.18 q_d, and 2.36 q_d, i.e., they exhibit a ratio of 1:2:4 with respect to the smallest observed wave number q_0. The higher spatial harmonics are primarily the effect of nonlinear optical properties of the pattern. Note that the y dimension, i.e., the wave vector, is perpendicular to $\mathbf{n}_0$. Thus longitudinal rolls, with a periodicity in the order of the cell gap, are represented.

C. Transition to normal rolls

The underlying mechanism of the longitudinal rolls is basically understood when one makes the assumptions of the model in Ref. [24]. Because they form in connection with a periodic director twist, we will refer to the respective experimental patterns as twist patterns, in order to distinguish them from other structures that are observed. With the investigated material, one can observe a frequency controlled transition from these twist longitudinal [TL, Figs. 6(a) and 7(a)] to

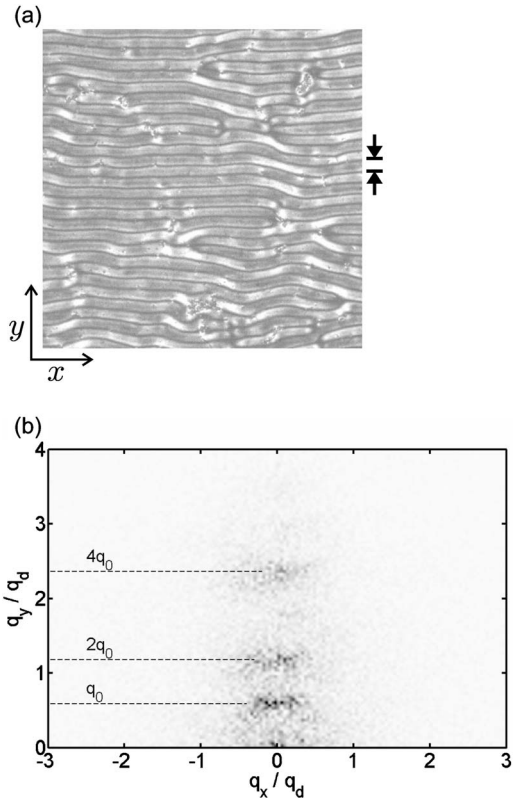

FIG. 6. Image under crossed polarizers, 640 μm $\times$ 640 μm (a) and Fourier spectrum of the corresponding image sequence (b), presented is the amplitude spectrum in the q_x, q_y space. Excitation frequency f_0=500 Hz, U=1.19 U_c, U_c=4.31 V, spatial reference wave number $q_d = 2\pi/d$ with the cell gap d=25 μm. The arrows in (a) mark the length d. $T - T_{iso} = -5$ K.

twist zigzag [TZ, Fig. 7(b)] and finally to twist normal rolls [TN, Fig. 7(c)] with respect to the initial director orientation $\mathbf{n}_0$. For a better optical contrast, the voltages in Fig. 7 have been chosen somewhat above the threshold. Except for different orientations, the optical appearance of the normal rolls resembles that of the longitudinal rolls. They are also interference patterns, near the threshold they are only visible between two polarizers. A modulated twist is necessary to produce the nonshadowgraph textures. Thus we classify them as twist patterns as well.

The dependence of the orientation of the convection rolls on frequency and voltage amplitude is depicted in Fig. 8. The orientation of the dashes corresponds to the orientation of the convection rolls with respect to $\mathbf{n}_0$. Each dash gives the primary orientation of the pattern wave vector determined at the respective frequency and voltage. The transition between twist longitudinal (TL) and twist normal patterns (TN) can be triggered by frequency changes. In the region below f_0 =3000 Hz, the longitudinal pattern dominates, whereas at higher frequencies (above 4500 Hz), the pattern sets in with normal rolls. The TL-TN transition with increasing frequency occurs across zigzag patterns (TZ). The left hand dash-dotted line in Fig. 8 marks the transition between twist longitudinal and twist zigzag rolls. The right hand one labels a frequency above which a qualitatively different regime occurs that will be referred to in the following as fluctuating

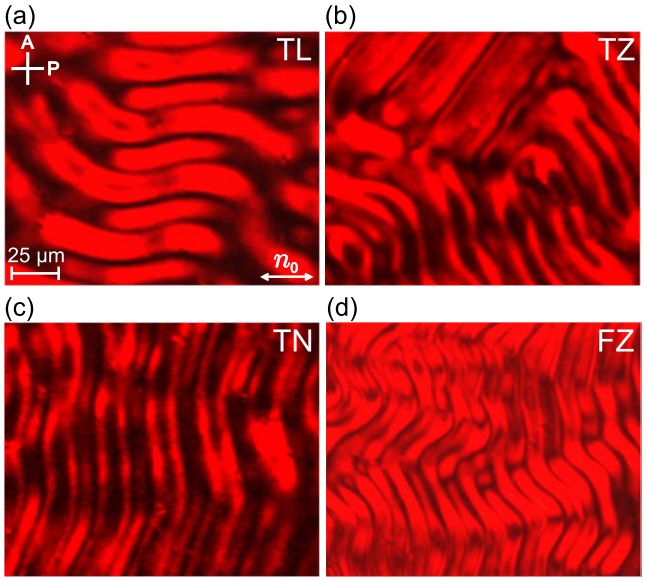

FIG. 7. (Color online) Convection rolls under crossed polarizers (P, A) and monochromatic light (632 nm) with increasing frequency. (a) twist longitudinal rolls (TL), f_0=1000 Hz, U=1.1 U_c, U_c=5.41 V, (b) twist zigzag rolls (TZ), f_0=3000 Hz, U=1.2 U_c, U_c=6.10 V, (c) twist normal rolls (TN), f_0=3650 Hz, U=1.1 U_c, U_c=6.96 V, (d) fluctuating zigzag patterns (FZ), f_0=6500 Hz, U =1.2 U_c, U_c=12.65 V. The orientation of the initial director $\mathbf{n}_0$ is marked.

zigzag patterns [FZ, see also Fig. 7(d)]. These patterns are localized, i.e., they do not develop uniformly in the cell plane but propagate with a sharp border to the nonconvecting state (Fig. 9). In the field of view they are visible without polarizers as shadowgraph structures [Fig. 9(a)]. The pattern is never spatially uniform but a rapid motion of convecting domains is observed. In order to decide whether the patterns are shadowgraph textures directly at onset, one has to look at

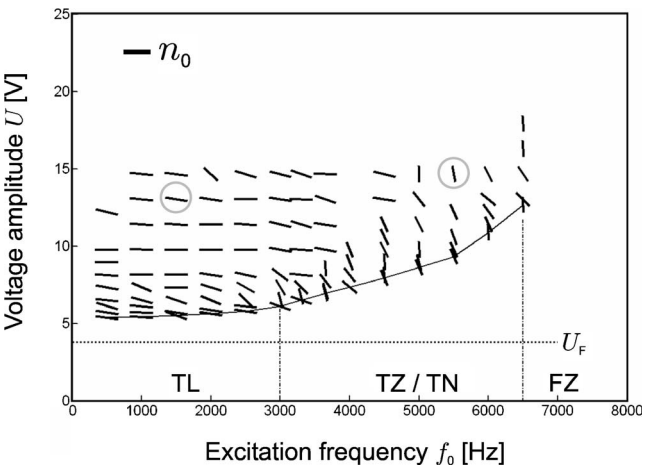

FIG. 8. Pattern state diagram. The orientation of the bars reflect the angle of the rolls with respect to $\mathbf{n}_0$. Transition frequencies are $f_0 \sim 3000$ Hz between TL and TZ rolls and f_0=6500 Hz between twist and FZ patterns. The threshold curve is plotted as solid line, U_F as dotted line. Grey circles mark the frequencies and voltage amplitudes corresponding to Figs. 11(a) and 11(b).

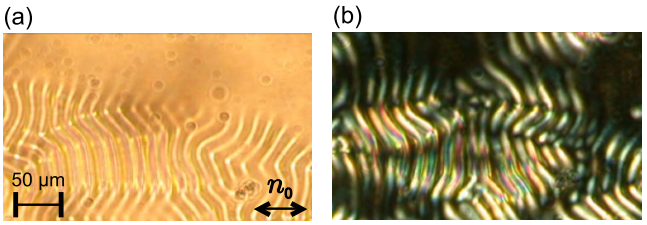

FIG. 9. (Color online) Images of fluctuating zigzag patterns. Same section without polarizers (a) and with crossed polarizers (b) near the threshold voltage at f_0=4000 Hz and U=16.3 V. Because a different cell has been used here, the frequency is not consistent with the respective range in Fig. 8.

the border of a patterned domain without polarizers and once again with two polarizers [Figs. 9(a) and 9(b), respectively]. This is practically impossible because the patterns fluctuate strongly and a statement about the optical appearance of the FZ convection rolls at onset cannot be made. The transition between the twist and the fluctuating zigzag pattern on the frequency axis is sharp. At still higher frequencies the pattern becomes gradually disordered even at the threshold and appears only in local spots. The splay Fréedericksz transition voltage U_F (dotted line in Fig. 8) is always below the threshold curve $U_c(f_0)$ (solid line) and does not have any detectable frequency dependence.

The wave number q_c (stars) near the threshold voltage U_c (circles) is shown in Fig. 10. In the TL and TZ regimes the wave number increases similar to U_c, whereas it remains nearly constant in the TN regime. At the transition frequency between TN and FZ patterns (right hand dashed-dotted line) the wave number jumps to higher values, i.e., a qualitative change between twist and fluctuating zigzag patterns occurs.

Figure 11 shows higher instabilities, i.e., patterns at voltages far from the threshold, in the twist longitudinal (a) and normal regimes (b) (pictures on the left hand side). Both patterns contain modes with a wave vector perpendicular to the original wave vector at the threshold, the roll orientations at threshold are sketched by the dashed lines. The superposition of two patterns is underlined by the modulus of the

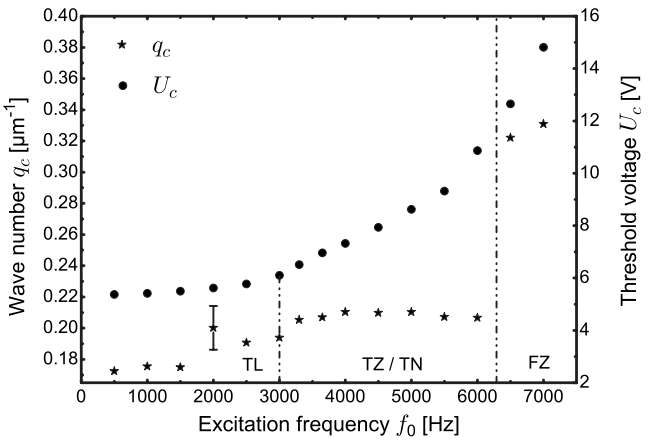

FIG. 10. Wave number q_c at $U \approx 1.05\ U_c$ (stars) and threshold voltage U_c (circles). The transitions between TL and TZ/TN as well as between twist and FZ patterns are marked by the dashed-dotted lines. The error of U_c is within symbol size.

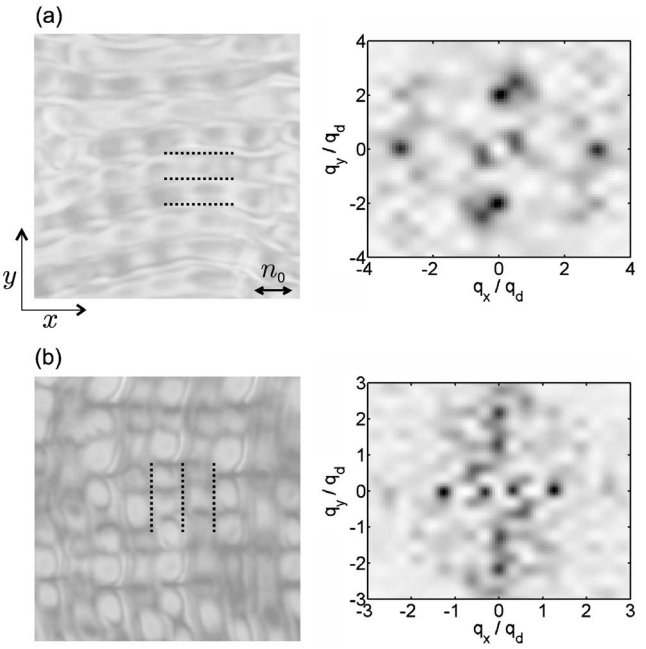

FIG. 11. Pictures of higher instabilities under monochromatic light (632 nm) at f_0=1500 Hz, U=2.37U_c, U_c=5.49 V (a) and f_0=5500 Hz, U=1.57U_c, U_c=9.32 V (b), left hand side. Frequencies and voltage amplitudes correspond to the grey circles in Fig. 8. Dotted lines sketch the roll orientation at threshold, direction of $\mathbf{n}_0$ is marked by the bar. Pictures are 50 μm×50 μm (a) and 80 μm×80 μm (b). Right hand side pictures show the 2D Fourier transforms of the images in the q_x, q_y space.

two-dimensional Fourier transforms of the pictures in the q_x, q_y space (right hand side in Fig. 11). The total intensity peaks at q_x=q_y=0 have been set to zero, the wave numbers have been scaled with q_d=2π/d. In both spectra, peaks occur on both spatial axes, i.e., observable spatial wave numbers exist in the x direction and the y direction as well. Cross peaks at the diagonals are not noticeable.

The transition frequency between twist patterns and fluctuating textures shifts with temperature. Figure 12 shows the angle of the convection rolls at the threshold voltage as a

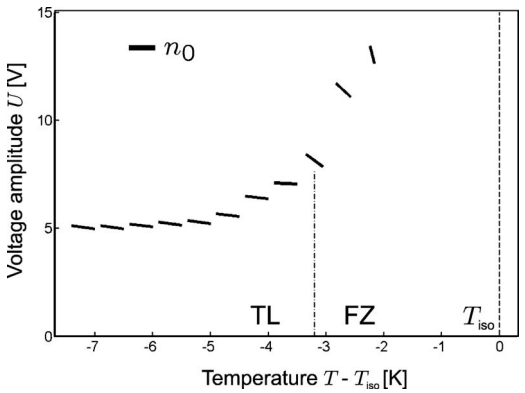

FIG. 12. Temperature dependent orientation of the convection rolls at the threshold voltage. Transition between TL and FZ rolls at $T-T_{iso}$=−3.2 K (dashed-dotted line). f_0=1 kHz, T_{iso} is marked by the dashed line.

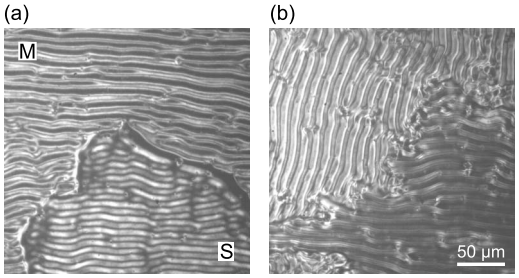

FIG. 13. Stable (S) and metastable (M) domain at $U=1.28U_c(M)$ (a) and $U=5.56U_c(M)$ (b), respectively. $U_c(M)=9$ V, $U_c(S)=10.5$ V. The white bar marks a length of 50 μm as well as the direction of $\mathbf{n}_0$ and the polarizer. The analyzer is aligned 90° with respect to the polarizer. $f_0=1$ kHz.

function of the temperature. A transition between twist longitudinal rolls and fluctuating zigzag patterns (dashed-dotted line) is observable, i.e., the transition frequency between twist and fluctuating rolls shifts towards lower values with increasing temperature. It can be excluded that the transition is affected by a sign inversion of $\Delta\sigma$ because the measurement of the effective conductivity σ_{eff} at different temperatures (Fig. 4) demonstrates that $\Delta\sigma_{\text{eff}}$ is negative in the relevant temperature range.

V. ELECTROCONVECTION ABOVE A NEW METASTABLE GROUND STATE

So far, different pattern regimes have been described that develop from the planar ground state after a splay Fréedericksz transition. But the investigated material exhibits still more exotic features. The formation of a second, metastable ground state is found when the cell has been exposed to electric fields of the order of 1 MV/m [25]. This ground state in absence of electric fields is optically different from the planar original ground state, and the effective birefringence is reduced by about 15%. It has been suggested that the material undergoes a phase transition from a uniaxial nematic phase into a biaxial nematic phase [36]. The metastable domains in the new ground state, denoted N_b in [36], are separated by a sharp boundary from the original (stable) domain. These domains can cover the whole cell plane, they relax at zero field to the original stable ground state within about one hour.

The appearance of the two types of domains was already mentioned in [25] and their optical and electrical properties have been described in detail in [36]. In Fig. 13, both domains, labeled S (stable) and M (metastable), coexist, separated by a sharp interface. In Fig. 13(a), the applied voltage is above the EHC threshold for both domains. Longitudinal rolls parallel to the initial director orientation $\mathbf{n}_0$ have formed. In Fig. 13(b), the convection rolls in the metastable domain have changed their orientation by about 90°. The contrast in the stable domain has become lower. Voltages $U_c(M)$ and $U_c(S)$ refer to the thresholds in the metastable and stable ground states, respectively, where the metastable ground state has the lower onset voltage for EHC. The two types of domains differ not only quantitatively in their EHC

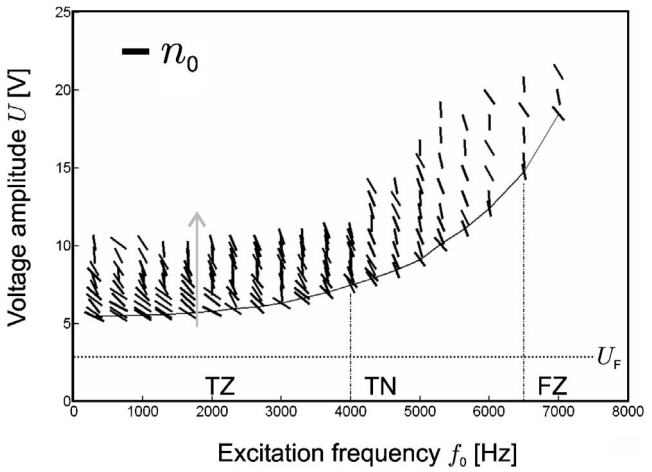

FIG. 14. Pattern state diagram for the metastable domain. Angle of bars reflect the orientation of the rolls with respect to $\mathbf{n}_0$. The transition frequencies between TZ and TN rolls ($f_0 \sim 4000$ Hz) as well as between TN and FZ rolls ($f_0 \sim 6500$ Hz) are marked by the dashed-dotted lines. The transition from TZ to TN rolls with increasing voltage is indicated by the grey arrow. The threshold curve is plotted as solid line, U_F as dotted line.

thresholds. There occurs also a qualitatively new property, a voltage dependent reorientation of the rolls, or rather a transition from twist longitudinal to twist normal rolls in the metastable domain. The transition from TZ to TN EHC can be seen in the pattern state diagram of Fig. 14, e.g., along the grey arrow. As in the structures described above, the transition to twist normal and fluctuating zigzag patterns takes place with increasing frequency. The pattern state diagram of Fig. 14 has been constructed from a different cell than that one used for Figs. 13 and 15. In this cell, slightly different threshold fields have been found. In particular, at the given temperature and excitation conditions, the TL rolls have not been observed at onset in this cell, but the pattern wave vector has always been in oblique orientation to the rubbing direction at frequencies below the TN regime. Again, the threshold curve (solid line) is always above the splay Fréedericksz transition voltage U_F (dotted line).

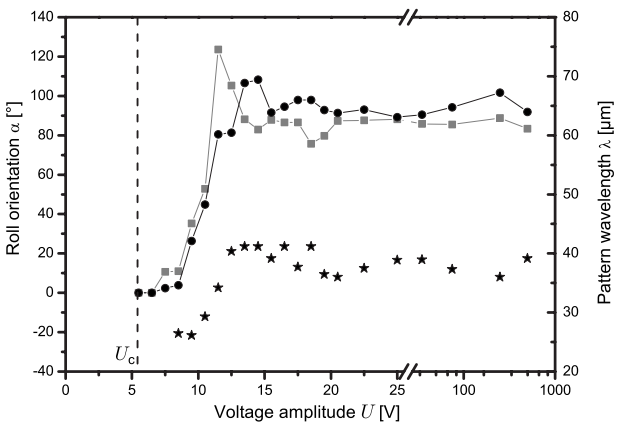

FIG. 15. Orientation of zig (circles) and zag rolls (squares) with respect to $\mathbf{n}_0$ in the metastable domain. Stars belong to the corresponding wavelengths. $f_0=1$ kHz.

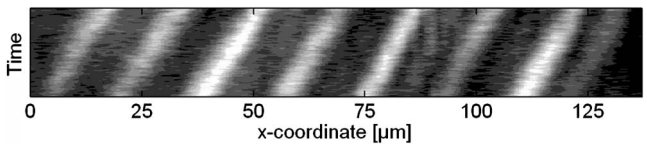

FIG. 16. Space-time-plot of the texture change in electroconvection patterns observed in a metastable domain. The time axis covers 6.7 s. $f_0=1.5$ kHz, $U=1.01U_c$, $U_c=7.66$ V. The spatial axis is a one-dimensional cross section of the texture, taken in the direction perpendicular to the roll orientation.

The voltage dependent pattern wave lengths (stars) and orientations α with respect to $\mathbf{n}_0$ (circles, squares) are depicted in Fig. 15. The convection rolls reorient from $\alpha=0°$ (longitudinal EHC) to $\alpha\approx 90°$ (normal EHC). In the intermediate range between both pattern regimes, the wave length increases rapidly with increasing roll deflection.

In contrast to the stable domain, the metastable domain forms traveling electroconvection rolls directly at onset, i.e., a Hopf bifurcation occurs in the (+,−) mesogen. The space-time plot of an image sequence near the threshold voltage is depicted in Fig. 16. From this, the velocity of the traveling convection rolls can be estimated to be 1.8 μm s^{-1}.

VI. DISCUSSION

In the experimental section, different pattern types have been described that are distinguished by their respective orientations of the convection rolls. Transitions between these patterns are observed for three different driving parameters, viz. frequency, voltage amplitude, and temperature. A short overview of the observed structures gives the following picture: When one starts from the planar ground state, the first instability is the uniform splay Fréedericksz transition at all frequencies and temperatures, all electroconvection patterns develop from the uniformly splay distorted ground state. At low frequencies and low temperatures, the patterns are longitudinal, i.e., wave vector and surface director $\mathbf{n}_0$ are perpendicular to each other. Above a certain frequency, a gradual rotation of the wave vector towards the $\mathbf{n}_0$ direction takes place, so that the rolls are finally aligned perpendicular to the director easy axis. None of these patterns is identical to the classical EHC because of the different optical appearance as interference pattern at onset.

The same orientational transition can be achieved when the temperature is changed, the longitudinal patterns appear at low temperatures. The temperature dependent threshold is somewhat counterintuitive, since one probably would expect that an increasing temperature lowers the characteristic times of the mesogenic material (lower director and charge relaxation times). Such a material parameter change at constant excitation frequency should be equivalent to a decrease of the excitation frequency at fixed temperature. We suggest that the reason for the temperature induced changes is the increasing distance from the lower temperature smectic phase which changes both the electric and conductivity anisotropies as well as some viscosities in some specific way.

At excitation voltages far above threshold, more complex patterns are observed, in particular, one finds a superposition of TN and TL to a kind of grid pattern. This is comparable to standard EHC, where a variety of patterns is formed. Their theoretical description requires a nonlinear analysis, which is beyond the scope of this paper. Moreover, the complexity of the patterns at onset increases at high frequencies (above $\approx$5 kHz). Since at low ac frequency, director and flow patterns are quasistationary and the charges are expected to alternate with the excitation frequency, it is most probable that the appearance of the fluctuating zigzags is related to the charge relaxation rate becoming equivalent to the excitation frequency.

Finally, we have described convection structures that develop from another, metastable, ground state (N_b) of the planar cell. The experimental situation is somewhat unsatisfactory, since the ground state has not been fully understood so far. Several possible explanations are given in Ref. [36]. After the application of high electric fields, the material becomes biaxial nematic, or at least it adopts a metastable director configuration that appears optically biaxial. In that new ground state N_b, one can reversibly generate a splay Fréedericksz transition, and one observes EHC patterns above that transition. We have included the description of these EHC patterns here since their optical characteristics is equivalent to that of the patterns in the original domains. On the other hand, one obvious qualitative difference is that TN rolls in the N_b domains travel at onset, whereas rolls in the original domains are stationary.

After this short classification, we now refer to the individual structures observed, discuss them in detail, and put them in the context of observations by other groups: A transition from longitudinal to normal rolls depending on the frequency has been found. In Refs. [28,29], a transition from normal to longitudinal rolls with increasing frequency has already been discovered in a temperature range, where the studied material undergoes a transition from $\Delta\sigma<0$ to $\Delta\sigma>0$. These patterns, observed in planar alignment, develop without a preceding Fréedericksz transition. The authors describe the frequency dependent transition from normal rolls (shadowgraph patterns at onset) to longitudinal rolls (no shadowgraph patterns at onset) as a transition from standard EHC (observable in pure (−,+) materials) to nonstandard electroconvection rolls, that are not explainable within the Carr-Helfrich model and its extensions [observable in (−,−) materials far from the transition to the (−,+) case]. In contrast, the compound studied here does not undergo a sign inversion of any of the anisotropies, hence, both transition mechanisms are not comparable.

The twist longitudinal as well as the twist normal patterns start with interference textures at onset. They produce shadowgraphs only at driving voltages several percent above the threshold. This leads to the presumption that both pattern types are related to structurally similar director fields and that they are driven by similar mechanisms. Moreover, the trend of the threshold curve and the frequency dependent wave number do not show any qualitative change at the transition between twist longitudinal, zigzag, and normal rolls. The model for the description of twist longitudinal rolls in [24] cannot predict a transition to the normal roll orientation. Moreover, it appears to be unlikely that the simplified mechanism that describes the longitudinal rolls can be easily

adapted to describe a change of the pattern wave vector with frequency, since no parameter in the model has a frequency dependence that could be responsible for such a transition. We note that the twist normal patterns are not simply equivalent to the well described conventional patterns, observed in standard experiments (−,+), because the TN rolls do not produce shadowgraph images at the pattern onset.

A transition from longitudinal to normal rolls with increasing voltage amplitude has been found in the metastable domain. Tóth-Katona *et al.* [29] already reported a transition between (longitudinal) nonstandard EHC to (normal) standard convection rolls as a function of the voltage amplitude in the (−,−) situation that cannot be compared with the (+,−) case.

A third transition that occurs with increasing temperature between twist and FZ patterns that appear to be shadowgraph patterns at threshold has been described here. Tóth-Katona *et al.* [29] describe a transition from parallel, nonstandard (no-shadowgraph) patterns to normal standard (shadowgraph) convection rolls at the transition temperature between the (−,−) and the (−,+) type of the mesogen. Indeed, this transition looks very similar to the twist pattern-FZ transition in our case, but our mesogen does not undergo a sign inversion either of the dielectric anisotropy or the conductivity anisotropy.

Remarkable is the particular structure of the patterns well above the threshold voltage where rolls with wave vectors in two orthogonal directions appear both in the twist longitudinal and twist normal regimes. Because the threshold curve does not show any qualitative change at intermediate frequencies between TL and TN patterns, the higher instability square patterns seem to be a superposition of both regimes.

Taking into account that the model in Ref. [24] has been derived without consideration of special molecular shapes, and considering further the similarity of TL rolls to observations reported in Ref. [23], we suggest that the observed transition effects do not result primarily from the specific bent-core shape of the molecules.

In conclusion, we have shown that novel types of electroconvection patterns can be found in a material with positive dielectric anisotropy and negative conductivity anisotropy, and that these patterns show previously unobserved optical and structural properties. The nature of the observed structural changes is not clear so far. It is to be expected that similar patterns play a role and have to be considered in the electro-optical application of similar types of materials, in particular bent-core nematics. The reason is that the parameter combination (+,−) seems to be much more common in bent-core nematics with their strong tendency to form layered structures. Such phases have been synthesized only recently, and they appear to be promising candidates for display and sensor materials, due to their unique material properties. They combine easy alignment and switchability of calamitic nematics with biaxial optical properties, potential polar effects and the existence of spontaneous electric polarizations, and consequently new types of electro-optic switching mechanisms. The understanding of the nature of electroconvection instabilities and conditions for their appearance in these materials appears to be essential for their further exploitation.

ACKNOWLEDGMENTS

Á. Buka, W. Pesch and T. John are cordially thanked for valuable discussions. J.H. acknowledges financial support by the state of Sachsen-Anhalt.

[1] L. Kramer and W. Pesch, in *Pattern Formation in Liquid Crystals*, edited by A. Buka and L. Kramer (Springer, New York, 1996), p. 221.
[2] A. Buka, N. Éber, W. Pesch, and L. Kramer, in *Self-Assembly, Pattern Formation and Growth Phenomena in Nano-Systems*, edited by A. A. Golovin and A. A. Nepomnyashchy (Springer, Secaucus, NJ, 2006), p. 55.
[3] S. Rasenat, G. Hartung, B. L. Winkler, and I. Rehberg, Exp. Fluids **7**, 412 (1989).
[4] E. Plaut, A. Joets, and R. Ribotta, J. Phys. III **7**, 2459 (1997).
[5] S. P. Trainoff and D. S. Cannell, Phys. Fluids **14**, 1340 (2002).
[6] U. Schneider, M. de la Torre Juarez, W. Zimmermann, and I. Rehberg, Phys. Rev. A **46**, 1009 (1992).
[7] H. Amm, M. Grigutsch, and R. Stannarius, Z. Naturforsch., A: Phys. Sci. **53**, 117 (1998).
[8] T. John, J. Heuer, and R. Stannarius, Phys. Rev. E **71**, 056307 (2005).
[9] I. Rehberg, S. Rasenat, J. Fineberg, M. de la Torre Juarez, and V. Steinberg, Phys. Rev. Lett. **61**, 2449 (1988).
[10] M. Dennin, M. Treiber, L. Kramer, G. Ahlers, and D. Cannell, Phys. Rev. Lett. **76**, 319 (1996).
[11] Martin Treiber, N. Éber, Á. Buka, and L. Kramer, J. Phys. (Paris), Colloq. **7**, 649 (1997).
[12] R. Ribotta, A. Joets, and L. Lei, Phys. Rev. Lett. **56**, 1595 (1986).
[13] W. Zimmermann and L. Kramer, Phys. Rev. Lett. **55**, 402 (1985).
[14] E. Plaut, W. Decker, and A. G. Rossberg, Phys. Rev. Lett. **79**, 2367 (1997).
[15] J.-H. Huh, Y. Hidaka, and S. Kai, Phys. Rev. E **58**, 7355 (1998).
[16] S. Rudroff, V. Frette, and I. Rehberg, Phys. Rev. E **59**, 1814 (1999).
[17] E. F. Carr, Mol. Cryst. Liq. Cryst. **7**, 253 (1969).
[18] W. Helfrich, J. Chem. Phys. **51**, 4092 (1969).
[19] E. Dubois-Violette, P. G. de Gennes, and O. Parodi, J. Phys. **32**, 305 (1971).
[20] E. Bodenschatz, W. Zimmermann, and L. Kramer, J. Physiol. (Paris) **49**, 1875 (1988).
[21] M. Treiber and L. Kramer, Mol. Cryst. Liq. Cryst. **261**, 311 (1995).
[22] Á. Buka, N. Éber, W. Pesch, and L. Kramer, Phys. Rep. **448**, 115 (2007).
[23] Á. Buka, B. Dressel, W. Otowski, K. Camara, T. Toth-Katona, L. Kramer, J. Lindau, G. Pelzl, and W. Pesch, Phys. Rev. E **66**, 051713 (2002).

[24] R. Stannarius and J. Heuer, Eur. Phys. J. E **24**, 27 (2007). Due to a scaling error, voltages given in Fig. 2 of this paper have to be divided by a factor of 2.88. This does not effect the results of this publication.
[25] M.-G. Tamba, W. Weissflog, A. Eremin, J. Heuer, and R. Stannarius, Eur. Phys. J. E **22**, 85 (2007).
[26] A. de Lózar Muñoz, T. Bock, M. Müller, W. Schöpf, and I. Rehberg, New J. Phys. **63**, 1367 (2003).
[27] B. Dressel and W. Pesch, Phys. Rev. E **67**, 031707 (2003).
[28] E. Kochowska, S. Németh, G. Pelzl, and Á. Buka, Phys. Rev. E **70**, 011711 (2004).
[29] T. Tóth-Katona, A. Cauquil-Vergnes, N. Éber, and Á. Buka, Phys. Rev. E **75**, 066210 (2007).
[30] D. Wiant, J. T. Gleeson, N. Éber, K. Fodor-Csorba, A. Jákli, and T. Tóth-Katona, Phys. Rev. E **72**, 041712 (2005).
[31] I. W. Stewart, *The Static and Dynamic Continuum Theory of Liquid Crystals* (Taylor and Francis, London, 2004).
[32] A. Krekhov, W. Pesch, N. Éber, T. Tóth-Katona, and Á. Buka, Phys. Rev. E **77**, 021705 (2008).
[33] S.-Q. Zhou, N. Éber, Á. Buka, W. Pesch, and G. Ahlers, Phys. Rev. E **74**, 046211 (2006).
[34] S.-Q. Zhou and G. Ahlers, Phys. Rev. E **74**, 046212 (2006), and refs. therein.
[35] A. Hertrich, W. Decker, W. Pesch, and L. Kramer, J. Phys. II **2**, 1915 (1992).
[36] R. Stannarius, A. Eremin, M.-G. Tamba, G. Pelzl, and W. Weissflog, Phys. Rev. E **76**, 061704 (2007).
[37] M.-G. Tamba, B. Kosata, K. Pelz, S. Diele, G. Pelzl, Z. Vakhovskaya, H. Kresse, and W. Weissflog, Soft Matter **2**, 60 (2006).
[38] H. Amm, R. Stannarius, and A. G. Rossberg, Physica D **126**, 171 (1999).
[39] H. Amm, M. Grigutsch, and R. Stannarius, Mol. Cryst. Liq. Cryst. **320**, 11 (1998).